COBEM 2021 26th International Congress of Mechanical Engineering
November 22-26, 2021, Virtual Congress, Brazil

COB-2021-0395
APPLICATION OF SDRE CONTROL TO HYBRID REMOTELY OPERATED VEHICLE

Allan C. F. de Oliveira
Reginaldo Cardoso
Decio C. Donha
University of Sao Paulo, 05508-010 São Paulo, SP, Brazil
allancfo@usp.br, reginaldo.cardoso@usp.br, decdonha@usp.br

Magno E. M. Meza
Federal University of ABC, 09210-580 Santo Andre, SP, Brazil
magno.meza@ufabc.edu.br

Abstract. *This paper presents a nonlinear dynamic model of a Hybrid Remotely Operated Vehicle described in the inertial frame, together with the control design based on the State-Dependent Riccati Equation method. Facing the mismatch that appears as a result of the extended linearization procedure of the vehicle dynamic, more specifically associated with the restoring force and moment vector, it is suggested to overcome this problem through the addition of a nonlinear compensator, which is calculated by the same weighting parameters assigned to the state error and control input. The designed controller is used in two scenarios: to drive the vehicle to the desired position and to perform a spiral movement, both with manually adjusted gains, each of them analyzed in the presence and absence of the disturbance vector. The proposed control responded appropriately to the selected tasks.*

Keywords: *HROV, Nonlinear dynamic model, State-Dependent Riccati Equation (SDRE), nonlinear compensator.*

1. INTRODUCTION

A Remotely Operated Vehicle (ROV) is a robot connected to a support vessel by means of umbilical cable that provides electrical power and telemetry, as well as transferring control signals given by the operator. With the discovery of the first deepwater oil field in 1975 [Zhang *et al.* (2019)], the oil industry led the research and improvement of ROV, which at first was exclusively applied to monitor marine habitat and to recover war material. Subsequently, this topic gained a lot of attention of the scientific community, expanding its application in various areas such as: oceanography; archeology and infrastructure.

The success of the original model enabled the development of its hybrid version, HROV. The term hybrid is associated with the vehicle's ability to move more than one way, i.e., navigation through thrusters and locomotion on some submerged structure and seabed through wheels (or track) [Cardoso *et al.* (2017)]. Given this feature, it is widely used for ship hull inspection.

The accuracy of the cited task depends on performing trajectory tracking or station keeping of the vehicle. This purpose is achieved by the control design, which presents two great difficulties inherent to the system: parametric uncertainty (as added mass, hydrodynamic coefficients, etc.) and significant disturbances of the environment in the form of underwater currents and interaction with waves [García-Valdovinos *et al.* (2014)].

Several studies are being carried out to describe increasingly detailed mathematical models and to design linear and nonlinear controllers for the position and attitude of submersibles, including: proportional-integral-derivative (PID)[Abidin *et al.* (2016)]; Fuzzy Logic [Johnson *et al.* (2016)][Aras *et al.* (2016)]; Model Predictive Control (MPC)[Molero *et al.* (2011)]; Sliding Mode Control (SMC) [Shekar *et al.* (2017)] or Second Order Sliding Mode Control (SOSMC) [Ismail and Putranti (2015)]; Feedback Linearization (FL) [Vervoort (2008)][Boehm *et al.* (2019)]; State-Depedent Riccati Equation (SDRE) [Yim and Oh (2003)][Naik and Singh (2007)][Geranmehr and Nekoo (2014)].

The SDRE methodology is recurrently applied in works over the last decades since it provides designers a very effective algorithm for synthesizing nonlinear feedback controls [Çimen (2008)] and offers many advantages compared with others nonlinear ones, among them [Cloutier and Stansbery (2002)]: to select design parameters, called weighting matrices, in such a way as to affect the performance of the closed-loop system; design flexibility related to nonuniqueness of state-dependent matrices; to impose hard bounds on the control or its respective rate; to preserve beneficial nonlinearities and to be directly applicable in nonminimum phase systems. The main step of this technique involves the transformation

of the nonlinear system into a linear-like structure which contains State-Dependent Coefficient (SDC) matrices, defined in literature as extended linearization or SDC parameterization [Çimen (2008)].

The existence of trigonometric functions of the system states (roll and pitch angle - ϕ and θ) in the hydrostatic moment and force vector (gravitational and buoyancy) prevents the factoring procedure of the ROV dynamic. A proposal suggested in [Yim and Oh (2003)] to overcome this problem would be to neglect the hydrostatic vector and to mitigate it by feedforward compensation in advance. For dealing with the diving control of the ROV, considering gravity and buoyancy force, in [Geranmehr and Nekoo (2014)] propose linearization with Taylor series expansion in order to include them into SDC matrix, along with the addition of the correction term analogous to sliding surface notion to conventional SDRE aiming perfect tracking. In [Naik and Singh (2007)] replace sine and cosine by (sinθ/θ)θ and ((cosθ -1)/θ)θ+1, respectively, thus allowing theirs incorporation into the SDC form. Unlike the aforementioned proposals, during the design of the SDRE control, we take into account the hydrostatic vector as a vehicle disturbance, which results in a nonlinear compensator whose gain is directly related to the same weighting parameters assigned to the state error and control input.

This paper presents the nonlinear dynamic model for the fully actuated HROV, assuming that all states are known. It is organized as follows: Section 2 presents the definitions and equations of the HROV dynamic; Section 3 describes the main points of the SDRE theory; Section 4 shows the results of the simulations and finally, the conclusions are presented.

2. MATHEMATICAL MODEL

The description of the movement of underwater vehicle in three-dimensional space requires 6 degrees of freedom (DOF) and introduction of two coordinate systems. According to [Fossen (2011)], the first one is located at sea level whose axes x_{EF}, y_{EF} and z_{EF} point to the north and east geographic, and the center of the Earth, respectively, identified as Earth Frame (EF) or inertial one. The second coordinate system is fixed on the body, named Body Frame (BF) or mobile one, and its axes are generally defined as: longitudinal x_{BF}, directed to the front of the vehicle, transversal y_{BF}, pointing to the right of the physical structure and normal z_{BF}, vertically downward. By the convention, Society of Naval Architects and Marine Engineers (SNAME) set linear (u, v e w) and angular (p, q and r) velocities, as well as forces (X, Y and Z) and moments (K, M and N) in BF, relative to location of sensors and thrusters. While the position (x, y and z) and the orientation (ϕ, θ and ψ) are mentioned in EF, where trajectory planning takes place. Figure 1 illustrates the representation of both systems and DOF. These variables are grouped as follows:

$$\boldsymbol{\nu} = [\boldsymbol{\nu_1} \quad \boldsymbol{\nu_2}]^T = [u \quad v \quad w \quad p \quad q \quad r]^T \qquad (\boldsymbol{\nu_1}, \boldsymbol{\nu_2} \in \mathcal{R}^3), \tag{1}$$

$$\boldsymbol{\eta} = [\boldsymbol{\eta_1} \quad \boldsymbol{\eta_2}]^T = [x \quad y \quad z \quad \phi \quad \theta \quad \psi]^T \qquad (\boldsymbol{\eta_1}, \boldsymbol{\eta_2} \in \mathcal{R}^3), \tag{2}$$

$$\boldsymbol{\tau} = [X \quad Y \quad Z \quad K \quad M \quad N]^T. \tag{3}$$

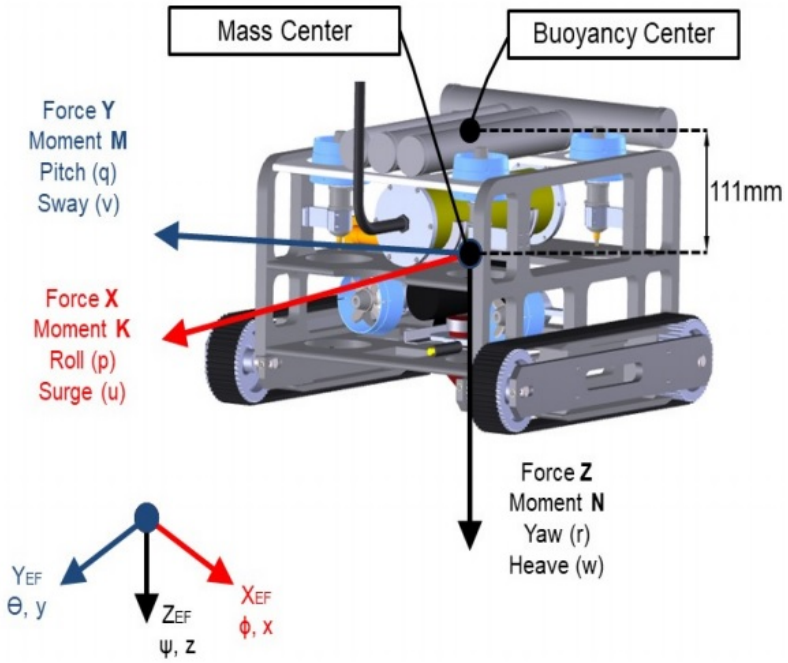

Figure 1. Degrees of freedom of the Proteo HROV.

The projection of a vector from EF to BF, and its reciprocity, results from the multiplication by a rotation. In several bibliographies, e.g. [Molero *et al.* (2011)],[Boehm *et al.* (2019)] and [Geranmehr and Nekoo (2014)], the Euler angle transformation is selected. Thus the relations of linear and angular velocities between coordinate systems can be announced as:

$$\dot{\boldsymbol{\eta}} = \mathbf{J}(\boldsymbol{\eta_2})\boldsymbol{\nu}, \tag{4}$$

such that $\mathbf{J}(\boldsymbol{\eta_2})$ is the Jacobian matrix of the system transformation

$$\mathbf{J}(\boldsymbol{\eta_2}) = \begin{bmatrix} \mathbf{J_1}(\boldsymbol{\eta_2}) & \mathbf{0_{3\times 3}} \\ \mathbf{0_{3\times 3}} & \mathbf{J_2}(\boldsymbol{\eta_2}) \end{bmatrix} \tag{5}$$

where

$$\mathbf{J_1}(\boldsymbol{\eta_2}) = \begin{bmatrix} C_\psi C_\theta & C_\psi S_\theta S_\phi - S_\psi C_\phi & C_\psi S_\theta C_\phi + S_\psi S_\phi \\ S_\psi C_\theta & S_\psi S_\theta S_\phi + C_\psi C_\phi & S_\psi S_\theta C_\phi - C_\psi S_\phi \\ -S_\theta & C_\theta S_\phi & C_\theta C_\phi \end{bmatrix} \quad \mathbf{J_2}(\boldsymbol{\eta_2}) = \begin{bmatrix} 1 & S_\phi T_\theta & C_\phi T_\theta \\ 0 & C_\phi & -S_\phi \\ 0 & S_\phi/C_\theta & C_\phi/C_\theta \end{bmatrix} \tag{6}$$

being $S_\alpha = sin(\alpha)$, $C_\alpha = cos(\alpha)$ and $T_\alpha = tan(\alpha)$.

Although the parameterization of the attitude by Euler's angles is intuitive, it verifies that $\mathbf{J_2}(\boldsymbol{\eta_2})$ is singular when $\theta = \pm 90^\circ$ consequently there is a loss of degree of freedom, phenomenon called Gimbal Lock. Due to the vehicle's operating purpose, this orientation is not desired, however if there was a need to act close to the singularity range, one could choose one of the two alternatives: the first option, using rotational matrices with different singularity points, so they will simply be avoided by alternating between transformations ($\mathbf{J_2}(\boldsymbol{\eta_2}) \leftrightarrow \mathbf{J_3}(\boldsymbol{\eta_2})$)[Okasha and Newman (2009)]. The second one involves rewriting the system orientation through quaternions [Zeng *et al.* (2015)].

The dynamic equation of the HROV expressed in the Body-fixed frame are given as follows [Fossen (2011)]:

$$\mathbf{M}\dot{\boldsymbol{\nu}} + \mathbf{C}(\boldsymbol{\nu})\boldsymbol{\nu} + \mathbf{D}(\boldsymbol{\nu})\boldsymbol{\nu} + \mathbf{g}(\boldsymbol{\eta_2}) = \boldsymbol{\tau} + \boldsymbol{\Delta}\mathbf{f} \tag{7}$$

where the matrix $\mathbf{M}$ represents the sum of the rigid-body and added mass inertia matrix; $\mathbf{C}(\boldsymbol{\nu})$ is the sum of rigid body and added mass Coriolis-centripetal matrix; $\mathbf{D}(\boldsymbol{\nu})$ denotes the hydrodynamic damping; $\mathbf{g}(\boldsymbol{\eta_2})$ is the resultant vector between gravitational and buoyancy forces; $\boldsymbol{\tau}$ refers to the control force and moment vector and $\boldsymbol{\Delta}\mathbf{f}$ the disturbance vector. Some simplifications are based on most of the hypotheses portrayed in the published works: the origin of the BF is coincident with the center of mass; the HROV has an approximately symmetrical geometric configuration in all planes; the parameters of the rigid-body inertia and added mass matrix are constant, and the inertia tensor is a diagonal matrix. The development of Eq. (7) and the vehicle's parameters can be seen in the Appendix.

The dynamic model in the Earth-fixed frame can be obtained by the time derivative of the Eq. (4)

$$\ddot{\boldsymbol{\eta}} = \dot{\mathbf{J}}(\boldsymbol{\eta_2})\boldsymbol{\nu} + \mathbf{J}(\boldsymbol{\eta_2})\dot{\boldsymbol{\nu}}, \tag{8}$$

and by the manipulation of Eq. (4) and (7) to replace $\boldsymbol{\nu}$ and $\dot{\boldsymbol{\nu}}$ in Eq. (8), which leads to:

$$\ddot{\boldsymbol{\eta}} = (-\mathbf{J}\mathbf{M}^{-1}(\mathbf{C}+\mathbf{D})\mathbf{J}^{-1} + \dot{\mathbf{J}}\mathbf{J}^{-1})\dot{\boldsymbol{\eta}} + \mathbf{J}\mathbf{M}^{-1}(\boldsymbol{\tau}+\mathbf{d}) \tag{9}$$

with $\mathbf{d} = \boldsymbol{\Delta}\mathbf{f} - \mathbf{g}$. Equivalently, the general state-space representation is:

$$\dot{\mathbf{x}}(t) = \mathbf{f}(\mathbf{x}(t), \mathbf{u}(t), \mathbf{d}(t)) \tag{10}$$

$$\mathbf{y}(t) = \mathbf{C}\mathbf{x}(t) \tag{11}$$

where $\mathbf{x} = [x \quad \dot{x} \quad y \quad \dot{y} \quad z \quad \dot{z} \quad \phi \quad \dot{\phi} \quad \theta \quad \dot{\theta} \quad \psi \quad \dot{\psi}]$ is the state vector, $\mathbf{u} = \boldsymbol{\tau}$ the control inputs, $\mathbf{y}$ output vector with all states acessible ($\mathbf{C} = \mathbf{I}_{12\times 12}$)

3. SDRE CONTROLLER

The SDRE approach deals with the optimal control problem for nonlinear system factoring it in the linear form with explicit matrices of the current states, $\mathbf{f}(\mathbf{x}) = \mathbf{A}(\mathbf{x})\mathbf{x}$, such that

$$\dot{\mathbf{x}}(t) = \mathbf{f}(\mathbf{x}(t), \mathbf{u}(t), \mathbf{d}(t)) \equiv \mathbf{A}(\mathbf{x})\mathbf{x} + \mathbf{B}(\mathbf{x})\mathbf{u}(t). \tag{12}$$

Such linearization will always exist, if the conditions on $\mathbf{f}(\mathbf{x})$ are satisfied: $\mathbf{f}(.) \in \mathcal{C}^1(\Omega)$ and $\mathbf{f}(\mathbf{0}) = \mathbf{0}$ [Çimen (2008)]. According to Fossen (2011), the matrix $\mathbf{C}$ has different parameterizations as long as it is antisymmetric, therefore it limits the choices of $\mathbf{A}(\mathbf{x})$, each one providing a different performance for the controller.

In this paper, the control objective is to track the desired output vector $\mathbf{z}$(t) while the energy cost is as low as possible, thus a performance index properly proposed would be

$$\mathcal{J}(\mathbf{e}(t),\mathbf{u}(t)) = \frac{1}{2}\int_0^\infty (\mathbf{e}(t)^T\mathbf{Q}(\mathbf{x})\mathbf{e}(t) + \mathbf{u}(t)^T\mathbf{R}(\mathbf{x})\mathbf{u}(t))dt, \tag{13}$$

where $\mathbf{e}(t) = \mathbf{z}(t) - \mathbf{C}\mathbf{x}(t)$ and the state and input weighting matrices, $\mathbf{Q}(\mathbf{x})$ and $\mathbf{R}(\mathbf{x})$ respectively, are parameters design that must satisfy requirements: $\mathbf{Q}(\mathbf{x}) \geq 0$ and $\mathbf{R}(\mathbf{x}) > 0$ [Çimen (2008)]. From Eq. (13), the Hamiltonian of the suboptimal control problem is given by:

$$H(\mathbf{x}(t),\mathbf{u}(t),\boldsymbol{\lambda}(t)) = \frac{1}{2}(\mathbf{z}(t)-\mathbf{C}\mathbf{x}(t))^T\mathbf{Q}(\mathbf{x})(\mathbf{z}(t)-\mathbf{C}\mathbf{x}(t))+\frac{1}{2}\mathbf{u}^T(t)\mathbf{R}(\mathbf{x})\mathbf{u}(\mathbf{t})+\boldsymbol{\lambda}^T(t)(\mathbf{A}(\mathbf{x})\mathbf{x}+\mathbf{B}(\mathbf{x})\mathbf{u}(t)) \tag{14}$$

such that $\boldsymbol{\lambda}(t)$ is a Lagrangian multiplier vector. The minimization of Eq. (13) is guaranteed through optimality conditions [Naidu (2003)]:

$$\frac{\partial H}{\partial \mathbf{u}} = 0; \quad \frac{\partial H}{\partial \boldsymbol{\lambda}} = \dot{\mathbf{x}}; \quad -\frac{\partial H}{\partial \mathbf{x}} = \dot{\boldsymbol{\lambda}}. \tag{15}$$

Expanding the optimality conditions and assuming that there is a linear transformation between the state and the costate ($\boldsymbol{\lambda}$) represented by

$$\boldsymbol{\lambda}(t) = \mathbf{P}(\mathbf{x})\mathbf{x}(t) - \mathbf{s}(t) \tag{16}$$

one can arrive at the following relations, as demonstrated in [Naidu (2003)]:

$$\dot{\mathbf{P}}(\mathbf{x}) = -\mathbf{P}(\mathbf{x})\mathbf{A}(\mathbf{x}) - \mathbf{A}^T(\mathbf{x})\mathbf{P}(\mathbf{x}) + \mathbf{P}(\mathbf{x})\mathbf{E}(\mathbf{x})\mathbf{P}(\mathbf{x}) - \mathbf{V}(\mathbf{x}) \tag{17}$$

and

$$\dot{\mathbf{s}}(t) = (\mathbf{P}(\mathbf{x})\mathbf{E}(\mathbf{x}) - \mathbf{A}^T(\mathbf{x}))\mathbf{s}(t) - \mathbf{W}(\mathbf{x})\mathbf{z}(t) + \mathbf{P}(\mathbf{x})\mathbf{d}(t), \tag{18}$$

where $\mathbf{E}(\mathbf{x}) = \mathbf{B}(\mathbf{x})\mathbf{R}^{-1}(\mathbf{x})\mathbf{B}^T(\mathbf{x})$, $\mathbf{V}(\mathbf{x}) = \mathbf{C}^T(\mathbf{x})\mathbf{Q}(\mathbf{x})\mathbf{C}(\mathbf{x})$ and $\mathbf{W}(\mathbf{x}) = \mathbf{C}^T(\mathbf{x})\mathbf{Q}(\mathbf{x})$. It is important to emphasize that the problem refers to the infinite horizon case ($t_f \to \infty$), so the solution of Eq. (17) converges to a constant value of $\mathbf{P}$, i.e., it becomes a solution of algebraic Riccati equation:

$$\mathbf{P}(\mathbf{x})\mathbf{A}(\mathbf{x}) + \mathbf{A}^T(\mathbf{x})\mathbf{P}(\mathbf{x}) - \mathbf{P}(\mathbf{x})\mathbf{E}(\mathbf{x})\mathbf{P}(\mathbf{x}) + \mathbf{V}(\mathbf{x}) = 0 \tag{19}$$

and Eq. (18) must be solved by backward integration in time, using the boundary condition: $\mathbf{P}(\mathbf{x}(t_f)) = \mathbf{0}$ and $\mathbf{s}(t_f) = \mathbf{0}$. An approximation of this solution is shown in [Çimen (2007)], also applied in [Prach and Tekinalp (2013)] and [Kuo and Wu (2016)], such that

$$\mathbf{s}(t) \approx (\mathbf{P}(\mathbf{x})\mathbf{E}(\mathbf{x}) - \mathbf{A}^T(\mathbf{x}))^{-1}(\mathbf{W}(\mathbf{x})\mathbf{z}(t) - \mathbf{P}(\mathbf{x})\mathbf{d}(t)). \tag{20}$$

The suboptimal control can be written as

$$\mathbf{u}(t) = -\mathbf{R}^{-1}(\mathbf{x})\mathbf{B}^T(\mathbf{x})\boldsymbol{\lambda}(t), \tag{21}$$

thus

$$\mathbf{u}(t) = \mathbf{K}(\mathbf{x})\mathbf{x}(t) + \mathbf{K}_\mathbf{z}(\mathbf{x})\mathbf{z}(t) + \mathbf{K}_\mathbf{d}(\mathbf{x})\mathbf{d}(t) \tag{22}$$

being:

$$\mathbf{K}(\mathbf{x}) = -\mathbf{R}^{-1}(\mathbf{x})\mathbf{B}^T(\mathbf{x})\mathbf{P}(\mathbf{x}) \tag{23}$$

$$\mathbf{K}_\mathbf{z}(\mathbf{x}) = \mathbf{R}^{-1}(\mathbf{x})\mathbf{B}^T(\mathbf{x})(\mathbf{P}(\mathbf{x})\mathbf{E}(\mathbf{x}) - \mathbf{A}^T(\mathbf{x}))^{-1}\mathbf{W}(\mathbf{x}) \tag{24}$$

$$\mathbf{K}_\mathbf{d}(\mathbf{x}) = -\mathbf{R}^{-1}(\mathbf{x})\mathbf{B}^T(\mathbf{x})(\mathbf{P}(\mathbf{x})\mathbf{E}(\mathbf{x}) - \mathbf{A}^T(\mathbf{x}))^{-1}\mathbf{P}(\mathbf{x}) \tag{25}$$

Figure 2 summarizes a general outline of the SDRE technique.

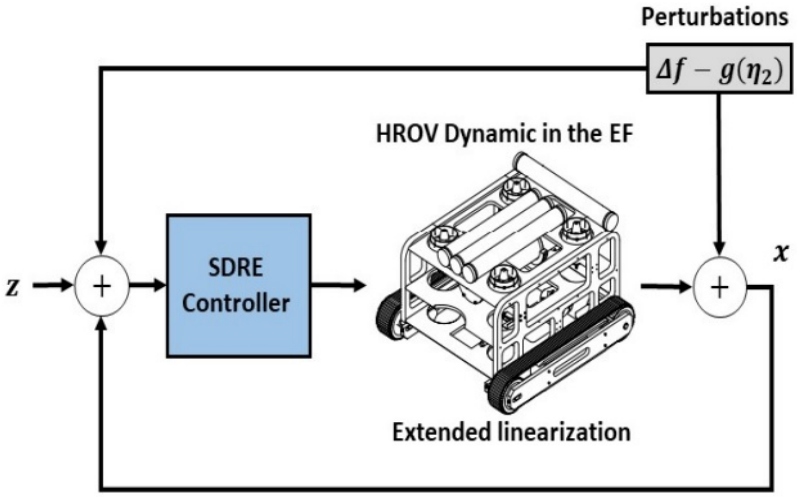

Figure 2. Layout of the control system and HROV dynamic.

4. SIMULATION

For the simulation, the numerical integrator used is the fourth order Runge-Kutta with time step of 0.01s. The control strategy was tested in two situations:

- Station keeping − to stay vehicle in position $x = 3$m, $y = 2$m and $z = 1$m;
- Tracking trajectory − to drive ROV in spiral movement with $\dot{z} = 0.1m/s$,

each of them were analyzed in two cases: absence and presence of the disturbance vector, which simulates the forces and moments from the ocean and the umbilical cable, see the Appendix.

4.1 Station Keeping

The design parameters of the control system are: $\mathbf{Q} = 100$ diag(10,1,10,1,10,1,10,1,10,1,10,1) and $\mathbf{R} = 0.1$ diag(1,1,1,1,1,1), without $\mathbf{\Delta f}$, $\mathbf{Q}$ = 1000000 diag(100,1,100,1,100,90,100,1,100,1,100,90) and $\mathbf{R}$ = 100 diag(0.1,0.1,0.1,1,1,1), with $\mathbf{\Delta f}$. The Fig.3 and Fig.4 show the HROV performance in reaching the desired linear and angular positions, while Fig.5 and Fig.6 illustrate the efforts of control.

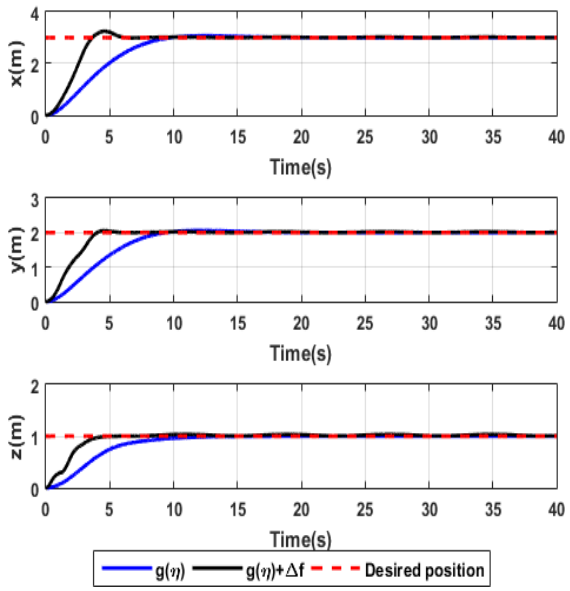

Figure 3. Linear position for station keeping.

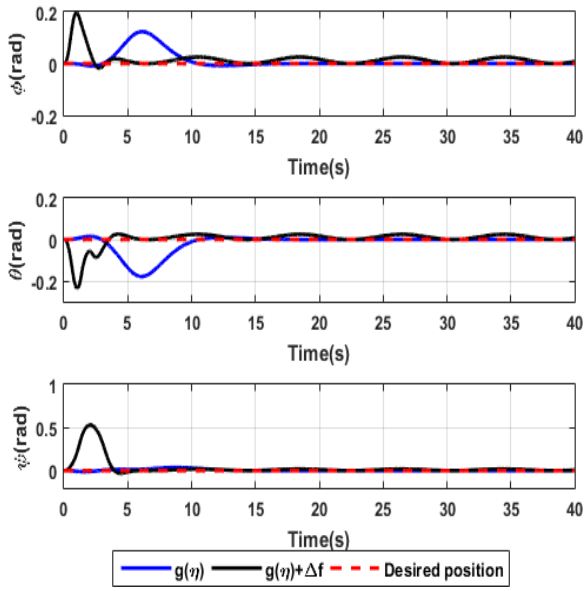

Figure 4. Angular position for station keeping.

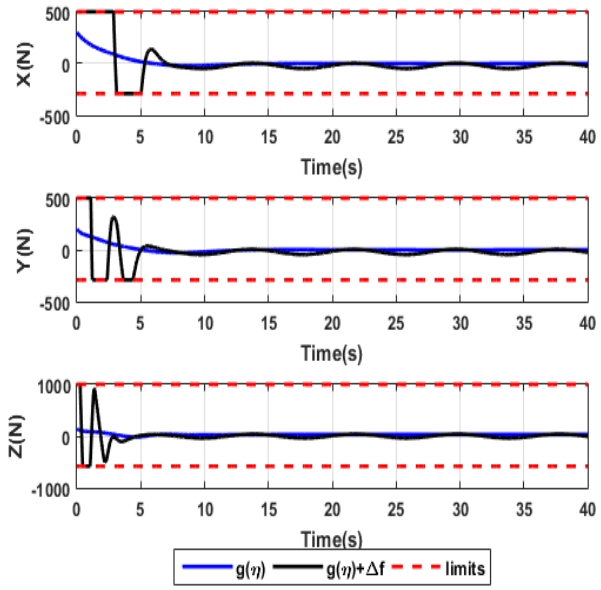

Figure 5. Force in the x, y and z directions for station keeping.

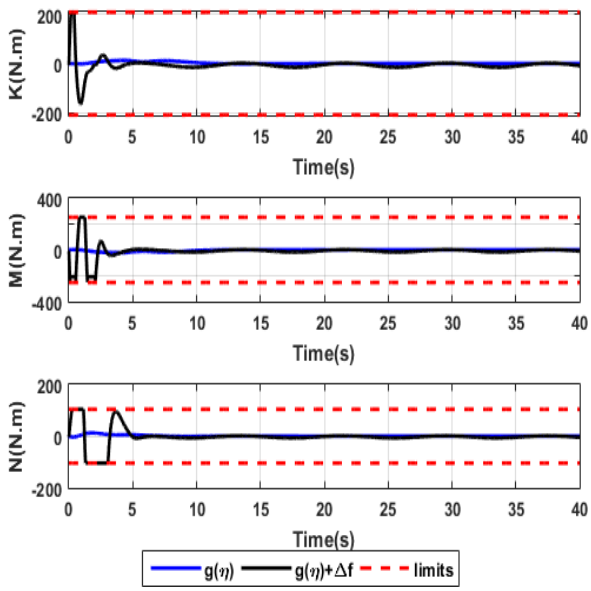

Figure 6. Moment in the x, y and z directions for station keeping.

In Figure 3, the rise times for the positions in the sinusoidal disturbance scenario ($\mathbf{\Delta f}$) are faster when compared to the absence of it. This can be explained by the fact that initially the disturbance acts in favor of the HROV displacement, on the other hand there is overshoot of the responses. In Figure 4, the angles oscillate around zero in the presence of waves and umbilical cable effect, unlike what can be seen when it is neglected. In figures 5 and 6, note that the forces and moments reach the limit values during the transient state for the case ($\mathbf{\Delta f}$). The quantification of the maximum errors in steady state (represented in percentage relative to the dimension of the vehicle - 705 mm of high, 852mm of width and 1076 mm of length) is shown in Tab.1.

Table 1. Maximum errors for station-keeping maneuver.

Position	g($\boldsymbol{\eta_2}$)	g($\boldsymbol{\eta_2}$) + $\mathbf{\Delta f}$
x	0	0.02m (2%)
y	0	0.02m(2%)
z	0	0.03m(4%)
ϕ	0	0.02 rad
θ	0	0.02 rad
ψ	0	0.02 rad

4.2 Spiral movement

The design parameters of the control system are: $\mathbf{Q}$ = 1000000 diag(950,1,950,1,120,90,9,1,9,1,40,9) and $\mathbf{R}$ = 100 diag(0.01,0.01,0.01,1,1,0.1), without $\mathbf{\Delta f}$, $\mathbf{Q}$ = 1000000 diag(950,1,950,1,120,90,9,1,9,1,40,9) and $\mathbf{R}$ = 100 diag(0.01,0.01, 0.01,1,1,0.1), with $\mathbf{\Delta f}$. In the XY plane, the circular trajectory executed by the HROV is parameterized as a function of time as follows

$$x = R\sin\left(\frac{\pi t}{30}\right) \quad y = R\cos\left(\frac{\pi t}{30}\right) \qquad (R = 5m) \tag{26}$$

Fig.7 and Fig.8 show the HROV performance in tracking the desired trajectory, while Fig.9 and Fig.10 illustrate the forces and moment generated by thrusters, that in this case its upper and lower limits have been removed to improve the viewing. The quantification of the maximum relative errors is shown in Tab. 2.

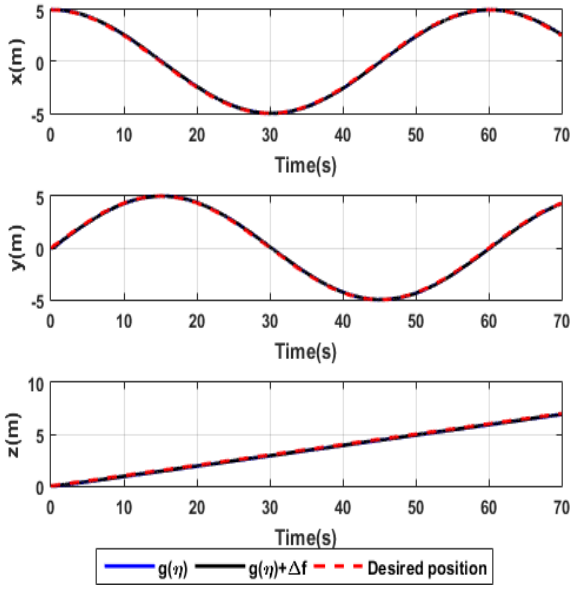

Figure 7. Linear position for trajectory tracking.

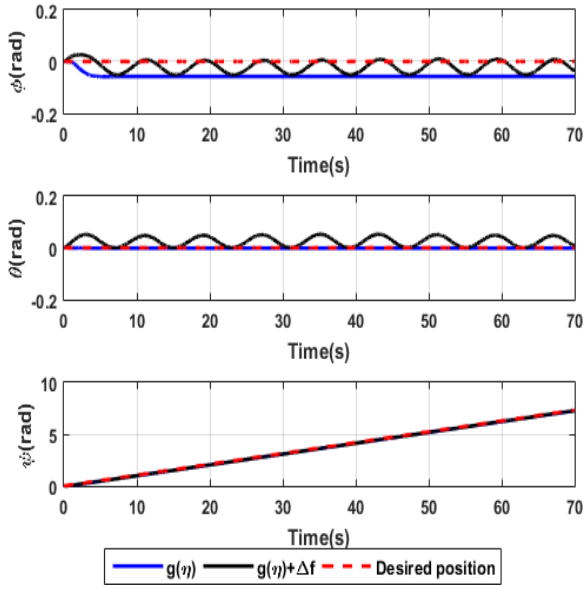

Figure 8. Angular position for trajectory tracking.

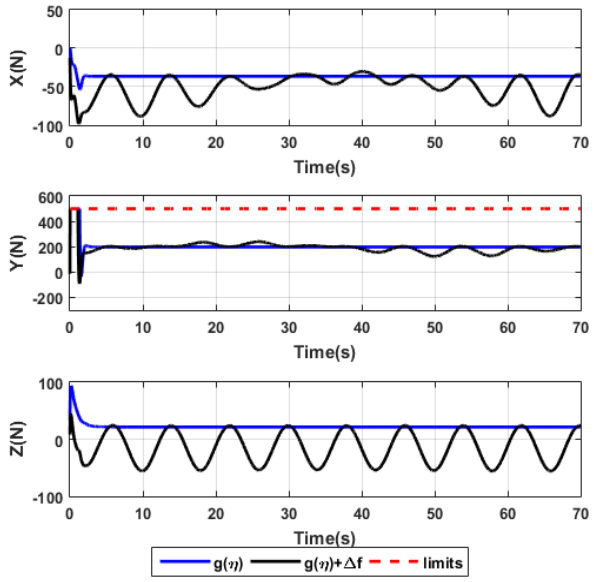

Figure 9. Force in the x, y and z directions for station keeping.

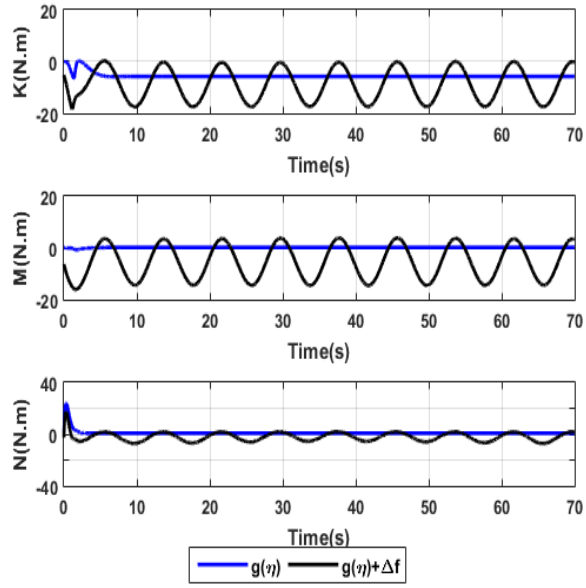

Figure 10. Moment in the x, y and z directions for station keeping.

Table 2. Maximum errors for Trajectory tracking.

Position	$g(\eta_2)$	$g(\eta_2) + \Delta f$
x	0.11m (10%)	0.11m (10%)
y	0.11m (13%)	0.11m (13%)
z	0.09m (13%)	0.09m (13%)
ϕ	0.07 rad	0.07 rad
θ	0	0.05 rad
ψ	0.09 rad	0.07 rad

5. CONCLUSION

In this paper, it was investigated the application of the State-Dependent Riccati Equation control for HROV considering a hard constraint on control and disturbance related to ocean waves and umbical cable, in order to obtain a practical design. The adopted strategy enables to encompass all the terms that cannot be placed into linear-like structure and treats them as a vehicle perturbations. Thus, there are no simplifications of these remaining nonlinear terms that may have a significant influence on the system response. Regarding errors, which are represented in percentage relative to the dimension of the vehicle, in the x-y-z positions are 2%, 2% and 4% for station keeping in presence of $\mathbf{\Delta f}$; 10%, 10% and 13% both without and with $\mathbf{\Delta f}$ for trajectory tracking, diverging the magnitude between forces and moments. The weighting matrices tuning process was done based on the analysis of simulations until an adequate solution was reached, giving higher priority to linear and angular positions. To get improvements in the results, this process can be accomplished through optimization such as hill climbing or genetic algorithms in future publications.

6. ACKNOWLEDGEMENTS

The authors would like to thank for the financial support made by the Coordenação do Aperfeiçoamento de Pessoal de Nível Superior – CAPES.

7. REFERENCES

Abidin, A.Z., Mardiyanto, R. and Purwanto, D., 2016. "Implementation of PID controller for hold altitude control in underwater remotely operated vehicle". In *2016 International Seminar on Intelligent Technology and Its Applications (ISITIA)*. Lombok, Indonesia.

Aras, M.S.M., Abdullah, S.S., Othman, S.Y.B., Sulaiman, M., Basar, M.F., Zambri, M.K.M. and Kamarudin, M.N., 2016. "Fuzzy logic controller for depth control of underwater remotely operated vehicle". *Journal of Theoretical and Applied Information Technology*, Vol. 91, No. 2, pp. 275–288.

Boehm, J., Berkenpas, E., Shepard, C. and Paley, D.A., 2019. "Feedback-linearizing control for velocity and attitude tracking of an rov with thruster dynamics containing input dead zones". In *2019 American Control Conference (ACC)*. Philadelphia, USA.

Cardoso, R., Meza, M.M.E., Rafikova, E. and Titotto, S.L.M.C., 2017. "Backstepping and integrative sliding mode control for trajectory tracking of a hybrid remotely operated vehicle". In *Proceedings of the IEEE International Conference on Robotics and Biomimetics*. Macau, China.

Cloutier, J.R. and Stansbery, D.T., 2002. "The capabilities and art of state dependent riccati equation-based design". In *Proceedings of the American Control Conference*. Anchorage, USA.

Ferreira, C.Z., 2016. *Tracking control system of the robot vehicle to inspection of submarine structures (in portuguese)*. Ph.D. thesis, University of ABC, Santo Andre, Brazil,l.

Fossen, T.I., 2011. *Handbook of marine craft hydrodynamics and motion control*. John Wiley & Sons Ltd, Chichester.

García-Valdovinos, L.G., Salgado-Jiménez, T., Bandala-Sánchez, M., Nava-Balanzar, L., Hernández-Alvarado, R. and Cruz-Ledesma, J.A., 2014. "Modelling, design and robust control of a remotely operated underwater vehicle". *International Journal of Advanced Robotic Systems*, Vol. 11, No. 1, pp. 1–16.

Geranmehr, B. and Nekoo, S.R., 2014. "The nonlinear suboptimal diving control of an autonomous underwater vehicle". In *Proceedings of the IEEE Second RSI/ISM International Conference on Robotics and Mechatronics (ICRoM)*. Tehran, Iran.

Çimen, T., 2007. "Approximate nonlinear optimal SDRE tracking control". *17th IFAC Symp. Automatic Control in Aerospace*, Vol. 40, No. 7, pp. 147–152.

Çimen, T., 2008. "State-dependent riccati equation SDRE control: A survey". In *Proceedings of the 17th IFAC World Congress*. Seoul, Korea.

Ismail, Z.H. and Putranti, V.W.E., 2015. "Second order sliding mode control scheme for an autonomous underwater vehicle with dynamic region concept". *Mathematical Problems in Engineering*, Vol. 2015, No. 2, pp. 1–13.

Johnson, J., Madhumitha, G., Yousuf, N. and Harikrishnan, S., 2016. "Design, development and fuzzy logic based control of a remotely operated underwater vehicle". In *Inernational Conference on Robotics and Automation for Humanitarian Applications (RAHA)*. Kollam, India.

Kuo, Y.L. and Wu, T.L., 2016. "A suboptimal tracking control approach based on the state-dependent riccati equation method". *Journal of Computational and Theoretical Nanoscience*, Vol. 13, No. 1, pp. 1013–1021.

Molero, A., Dunia, R., Cappelletto, J. and Fernandez, G., 2011. "Model predictive control of remotely operated underwater vehicles". In *2011 50th IEEE Conference on Decision and Control and European Control Conference*. Orlando, USA.

Naidu, D.S., 2003. *Optimal Control Systemsl*. CRC Press, Boca Raton, USA.

Naik, J.M.S. and Singh, S.N., 2007. "State-dependent riccati equation-based robust dive plane control of auv with control

constraints". *Ocean Engineering*, Vol. 34, No. 11-12, pp. 1711–1723.

Okasha, M. and Newman, B., 2009. "Switching algorithm to avoid attitude representation singularity". In *AIAA Atmospheric Flight Mechanics Conference*. Chicago, USA.

Prach, A. and Tekinalp, O., 2013. "Development of a state dependent riccati equation based tracking flight controller for an unmanned aircraft". In *AIAA Guidance, Navigation, and Control (GNC) Conference*. Boston, USA.

Shekar, S.C., Rao, B.V. and Rao, P.M., 2017. "Modelling and control of autonomous under water vehicle using sliding mode controller". *International Journal of Innovative Research in Electrical, Electronics, Instrumentation and Control Engineering*, Vol. 5, No. 6, pp. 235–239.

Vervoort, J.H.A.M., 2008. *Modeling and Control of an Unmanned Underwater Vehicle*. Ph.D. thesis, Master Program in Mechanical Engineering, University of Canterbury, Christchurch, New Zealandl.

Yim, S. and Oh, J., 2003. "A novel approach for the optimal control of autonomous underwater vehicles". *Control and Cybernetics*, Vol. 32, No. 1, pp. 127–146.

Zeng, Q., Zhang, M., Liu, H., Suil, X., Liang, S. and Song, Z., 2015. "Research of underwater navigation on a ROV with structure detection and decontamination". In *The 27th Chinese Control and Decision Conference (CCDC)*. Qingdao, China.

Zhang, G., Qu, H., Chen, G., Zhao, C., Zhang, F., Yang, H., Zhao, Z. and Ma, M., 2019. "Giant discoveries of oil and gas fields in global deepwaters in the past 40 years and the prospect of exploration". *Journal of Natural Gas Geoscience*, Vol. 4, No. 1, pp. 1–28.

8. APPENDIX

Table 3. PROTEO HROV's parameters [Ferreira (2016)].

Parameter	Value	Parameter	Value
m	142 Kg	X_u	-41.45 Kg/s
mg	1391.6 N	$X_{u\|u\|}$	-326.6 Kg/m
$\rho\Lambda g$	1424.92 N	Y_v	135.09 Kg/s
$X_{\dot{u}}$	-450.5 Kg	$Y_{v\|v\|}$	-1016.57 Kg/m
$Y_{\dot{v}}$	-500 Kg	Z_w	311.64 Kg/s
$Z_{\dot{w}}$	-550 Kg	$Z_{w\|w\|}$	-1706.55 Kg/m
I_x	20.48 Kg.m^2	K_p, M_q	-5 Kg.m^2/(s.rad)
I_y	19.79 Kg.m^2	$K_{p\|p\|}$	-200 Kg.m^2/rad^2
I_z	30.83 Kg.m^2	$M_{q\|q\|}$	-200 Kg.m^2/rad^2
$M_{\dot{q}}$	-200 Kg.m^2	N_r	-2.27 Kg.m^2/(s.rad)
$K_{\dot{p}}$	-200 Kg.m^2	$N_{r\|r\|}$	-111.5 Kg.m^2/rad^2
$N_{\dot{r}}$	-162 Kg.m^2	z_b	- 0.11 m

The matrices corresponding to the HROV dynamics are:

$$\mathbf{M} = diag\left[m - X_{\dot{u}} \quad m - Y_{\dot{v}} \quad m - Z_{\dot{w}} \quad I_x - K_{\dot{p}} \quad I_y - M_{\dot{q}} \quad I_z - N_{\dot{r}}\right],$$

$$\mathbf{C}(\boldsymbol{\nu}) = \begin{bmatrix} 0 & 0 & 0 & 0 & (m - Z_{\dot{w}})w & -(m - Y_{\dot{v}})v \\ 0 & 0 & 0 & -(m - Z_{\dot{w}})w & 0 & (m - X_{\dot{u}}) \\ 0 & 0 & 0 & (m - Y_{\dot{v}})v & -(m - X_{\dot{u}}) & 0 \\ 0 & (m - Z_{\dot{w}})w & -(m - Y_{\dot{v}})v & 0 & (I_z - N_{\dot{r}})r & -(I_y - M_{\dot{q}})q \\ -(m - Z_{\dot{w}})w & 0 & (m - X_{\dot{u}}) & -(I_z - N_{\dot{r}})r & 0 & (I_x - K_{\dot{p}})p \\ (m - Y_{\dot{v}})v & -(m - X_{\dot{u}}) & 0 & (I_y - M_{\dot{q}})q & -(I_x - K_{\dot{p}})p & 0 \end{bmatrix},$$

$$\mathbf{D}(\boldsymbol{\nu}) = -diag\left[X_u + X_{u|u|}|u| \quad Y_v + X_{v|v|}|v| \quad Z_w + Z_{w|w|}|w| \quad K_p + K_{p|p|}|p| \quad M_q + M_{q|q|}|q| \quad N_r + K_{r|r|}|r|\right],$$

$$\mathbf{g}(\boldsymbol{\eta_2}) = \begin{bmatrix} \sin(\theta)(mg - \rho\Lambda g) \\ -\cos(\theta)\sin(\phi)(mg - \rho\Lambda g) \\ -\cos(\theta)\cos(\phi)(mg - \rho\Lambda g) \\ -\rho\Lambda g(z_b\cos(\theta)\sin(\phi)) \\ -\rho\Lambda g(z_b\sin(\theta)) \\ 0 \end{bmatrix}.$$

The amplitudes of the disturbances are equals to 5% of the maximum propulsion or torque value and the frequency was used the same one of [Cardoso *et al.* (2017)][Ferreira (2016)], as follows,

$$\boldsymbol{\Delta}(\mathbf{f}) = \begin{bmatrix} 12.5 + 12.5\sin(0.785t)N \\ 12.5 + 12.5\sin(0.785t)N \\ 25 + 25\sin(0.785t)N \\ 5.2 + 5.2\sin(0.785t)N \\ 6.3 + 6.3\sin(0.785t)N \\ 2.6 + 2.6\sin(0.785t)N \end{bmatrix}.$$

9. RESPONSIBILITY NOTICE

The authors are solely responsible for the printed material included in this paper.